Phase Separation of Ultrahigh Molecular Weight Isotactic Polypropylene Solutions in the Gelation Process Estimated in Relation to the Morphology and Mechanical Properties of the Resultant Dry Gel Films

Masaru Matsuo* and Tomoko Hashida†

Department of Textile and Apparel Science, Faculty of Human Life and Environment, Nara Women's University, Nara 630-8506 Japan

Koji Tashiro*

Department of Macromolecular Science, Faculty of Science, Osaka University, Osaka 560-0043 Japan

Yasuyuki Agari

Osaka Municipal Technical Research Institute, Osaka 536-8553 Japan

Received August 6, 2001; Revised Manuscript Received December 21, 2001

ABSTRACT: The phase separation of ultrahigh molecular weight isotactic polypropylene (it-UHMWPP) solution in the gelation process was investigated by quenching the solutions to the desired temperature. When an incident beam of an He−Ne gas laser was directed to the gel, the logarithm of scattered intensity increased linearly with time in the initial stage and tend to deviate from this linear relationship in the later stage. The melting endotherm of the differential scanning calorimetry curve showed a clear peak in the later stage, but no peak could be observed in the initial stage, indicating poor ordering of molecules in polymer-rich phase. The scattered intensity of laser beam from the gel showed a peak in the scattering angle direction. The peak became more intense with increasing time, but the peak position did not change. Accordingly, the phase separation of UHMWPP solution in the initial stage was analyzed within the framework of the linear theory of spinodal decomposition. In parallel to this small-angle light-scattering experiment, the time-resolved measurements in the gelation process were carried out for X-ray diffraction and infrared and Raman spectra. These data could be interpreted reasonably in terms of formation of crystallites as cross-linkages of the gels. Under optical microscopy, it was confirmed that the gels prepared by quenching the solution to room temperature compose of periodic honeycomblike structure characterizing the spinodal decomposition of the solution due to thermodynamic instability. The average size of this periodic structure is slightly larger than that estimated from the scattering angle to give the maximum value of growth rate of concentration fluctuation. Periodic honeycomblike structure was also observed for the dry film under a scanning electron microscopy. The hole size of the honeycomblike structure became smaller as the quenching temperature decreased, and the size distribution was narrow. The dried films were stretched up to 60 times, as has been reported already. The possibility of successful elongation up to $\lambda = 60$ became higher with decreasing quenching temperature. Young's modulus, crystallinity, and molecular orientational degree of the resultant dry gel films became higher with decreasing hole size of honeycomblike structure. Accordingly, it turns out that the dense network structure created by the spinodal decomposition of the solution plays an important role in ensuring smooth transmission of inner stress in the stretching direction and ultradrawing of UHMWPP film can be achieved.

Introduction

It is well-known that the effective drawability of ultrahigh-molecular-weight polyethylene (UHMWPE)[1−5] and ultrahigh-molecular-weight polypropylene[6−7] (UHMWPP) is dramatically enhanced by elongation of specimens prepared by gelation/crystallization from semidilute solutions. It was found that for a sufficiently high molecular weight samples, the achievable maximum draw ratio depends principally on the concentration of the solution from which the gel is made. This phenomenon was attributed to a reduced number of entanglement meshes per molecule in solution−cast/spun polymers in comparison with those obtained from the melt.[2] A question arises as to whether the maximum draw ratio of the dry gel films depends on the gelation temperature associated with the phase separation of the solution and chain dynamics. To demonstrate it, Ogita et al.[8] prepared the gel of UHMWPE (average viscosity molecular weight $M_v = 3 \times 10^6$) by quenching the solution with a concentration of 0.6 g/100 mL to room temperature. This concentration corresponded to the optimum concentration to ensure maximum draw ratio of the resultant film, when the solution was quenched to room temperature (20 °C). According to that paper, hot UHMWPE solution was quenched at various temperatures beyond 20 °C, and then the solvent was evaporated at 20 °C. Young's modulus, tensile strength, crystallinity, and molecular orientation of the resultant films were less pronounced with increasing gelation/crystallization temperature. At 80 °C, the solution showed phase separation in macroscopic level and nonuniform gels appeared. The surface of the resultant film prepared by solvent evaporation was not smooth and the drawability was not significant. These phenom-

* To whom correspondence should be addressed.
† Present address: Department of Macromolecular Science, Faculty of Science, Osaka University, Osaka 560-0043 Japan.

10.1021/ma011402+ CCC: $22.00
Published on Web 03/08/2002

ena are thought to be due to the fact that the morphology of the dry gel film is intimately related to the temperature-dependent gelation mechanism of UHMWPE in solutions. As the preliminary experiments, the gelation mechanism of UHMWPE was investigated by a light-scattering measurement. However creative results could not be obtained because of the difficulty in measuring the scattered intensity with time, since the gels were not transparent. Because of transparent gels, UHMWPP was used in this paper instead of UHMWPE, to study gelation mechanism of the semidilute solutions which provide the greatest drawability of the resultant dry gel films. The kinetics of the gelation mechanism was analyzed in terms of phase separation of UHMWPP solution.

One of the typical physical gels of linear polymers has been observed for atactic (at-), isotactic (it-), and syndiotactic (st-) polystyrene (PS).[9−11] Tan et al. demonstrated the gel formation of at-PS solution and proposed the phase diagram by considering molecular weight and solvents.[12] Guenet et al. provided a coherent explanation for the so-called "enhanced low-angle scattering (ELAS)" observed in moderately concentrated solutions[13−15] and proposed a formation of complex between at-PS and carbon disulfide (CS_2) complex or a stoichiometric compound based on the results of differential scanning calorimetry (DSC).[16] To justify their results for the ELAS, they pointed out that CS_2 behaves as a good solvent for at-PS at room temperature, which is in contradiction with the hypothesis by Boyer et al.[17] However, recent studies concerning the temperature dependence of Kratky plots for the at-PS and CS_2 systems proved that CS_2 behaves as a good solvent for at-PS at room temperature but as a poor solvent at temperatures <-30 °C.[18]

On the other hand, gel structure and dynamics of it-PS and st-PS have been investigated in their equilibrium states. The studies of it-PS have been carried out by using *cis*-decalin as solvent to analyze the coagulation structure as well as the conformation of an isolated chain in gels relating to a 3_1 helix. For st-PS gels, Kobayashi et al.[7−11] pointed out that there exist long chains with TTGG conformation within the gels at room temperature, and the further analysis of st-PS gels prepared by several solvents was done on the basis of the results of Kratky plots and the time dependence of the invariant of the small-angle neutron scattering data. As for the results, it was found that the molecular coagulation process is sensitive to the kind of solvent.

In any case, there exist few reports for time dependence of gel formation of crystalline polymers. Recently the gelation process of poly(vinylidene fluoride)−organic solvent system was investigated as a function of time by Tashiro et al.[19] with Fourier transform infrared spectroscopy. In the present paper, gel formation of it-UHMWPP will be investigated in terms of phase separation of the solution due to thermodynamic instability. In doing so, the time dependence of gel formation has been estimated in macroscopic and microscopic levels by using elastic light scattering, X-ray diffraction, optical microscopy, scanning electron microscopy, and infrared and Raman spectroscopy. This is the first report to trace the gel formation mechanism of the it-UHMWPP solution as long as the authors have been investigating the literature. Certainly, the greatest drawability of UHMWPE and UHMWPP has been estimated in terms of significant crystal transition from a folded to a fibrous type[3] as well as the concentration of solution.[2] However, a gel formation process by quenching the solution has never been reported.

The main focus of this paper is to investigate the formation process of UHMWPP gels. The analysis is pursued in terms of liquid−liquid phase separation of solution by concentration fluctuation. This information is thought to be quite important for understanding the structure and mechanical property of the resultant dry gel film.

Experimental Section

Sample Preparation of Dry Gel Films. It-polypropylene with an average viscosity molecular weight of 5.4×10^6g/mol was used as a test specimen. The specimen was furnished by Mitsui-Chemical Inc. A *cis*-decalin solution containing 0.4 g/100 mL of UHMWPP and 0.1 w/w% of antioxidant di-*tert*-*p*-cresol was prepared by heating the well-blended polymer/solvent mixture at 160 °C for 40 min under nitrogen atmosphere. Through preliminary experiments, it has been found that the concentration of 0.4 g/100 mL ensures the greatest significant drawability of the resultant dry gel film prepared by gelation/crystallization at 0 °C and evaporating solvent at 20 °C.[20−21] The elongation was done in a hot oven at 150 ∼ 170 °C under nitrogen gas. The possibility of successful drawing up-to-draw ratio $\lambda = 60$ becomes lower as the concentration moves away from 0.4 g/100 mL. The hot homogenized solution with the concentration of 0.4 g/100 mL was quenched by pouring into an aluminum tray that was surrounded by a poly(ethylene glycol) (PEG) bath at the desired temperatures, 30, 50, and 60 °C, and the resultant gel was maintained at the same temperature for 12h without evaporating solvents. After that, the decalin was allowed to evaporate from the gels under ambient conditions. The possibility of successful elongation up to $\lambda = 60$ became higher with decreasing quenching temperature. The resulting 300 μm thick dry gel film was immersed in ethanol and subsequently air-dried to remove residual traces of the decalin−ethanol mixture. The specimens were characterized by density, wide-angle X-ray diffraction (WAXD), scanning electron microscopy (SEM), and diffraction scanning calorimetry (DSC).

Observation of Phase Separation of it-UHMWPP Solutions. For the investigation of phase separation of the solution, UHMWPP with $\bar{M}_v = 2.5 \times 10^6$ was employed, since in the case of UHMWPP with $\bar{M}_v = 5.4 \times 10^6$ the phase separation by gelation was too rapid to detect the scattered intensity as a function of time by elastic light scattering. The solutions with various concentrations were prepared at 160 °C. They were put in each test tube and kept at 100 °C for 5 min to avoid a drastic convection. After that the test tube was immediately set in a time-resolved light-scattering instrument, the measurements were done at desired temperature beyond 50 °C by using an He−Ne gas laser. The diameter of the light-scattering cell tube was 10 mm to maintain the equilibrium state in solution ensuring the construction of the ergodic hypothesis.

The structure evolution of gels with time was also estimated by WAXD. Time-resolved X-ray scattering measurement was carried out with Cu Kα radiation by using a CCD camera (C4880, Hamamatsu Photonics Co., Ltd.) to trace the gelation process by quenching the solution from 150 °C to room temperature, in which the sample to camera distance was set to 70 mm and the collimator was 0.5 mm in diameter. The heating process of gel was estimated by measuring the X-ray scattering intensity with Mo Kα radiation by using the DIP-1000 system of MAC Science Co., Ltd. The diffraction intensity was accumulated for 30 min at each temperature. The diameter of X-ray capillary was 1 mm.

The FT-IR spectra were measured by using a BioRad FTS60A FTIR spectrometer. The gel was sandwiched between a pair of KBr plates and heated to 150 °C. After being kept for 5 min at 150 °C, the gels were cooled to room temperature immediately by flowing air. The change in the FT-IR spectra

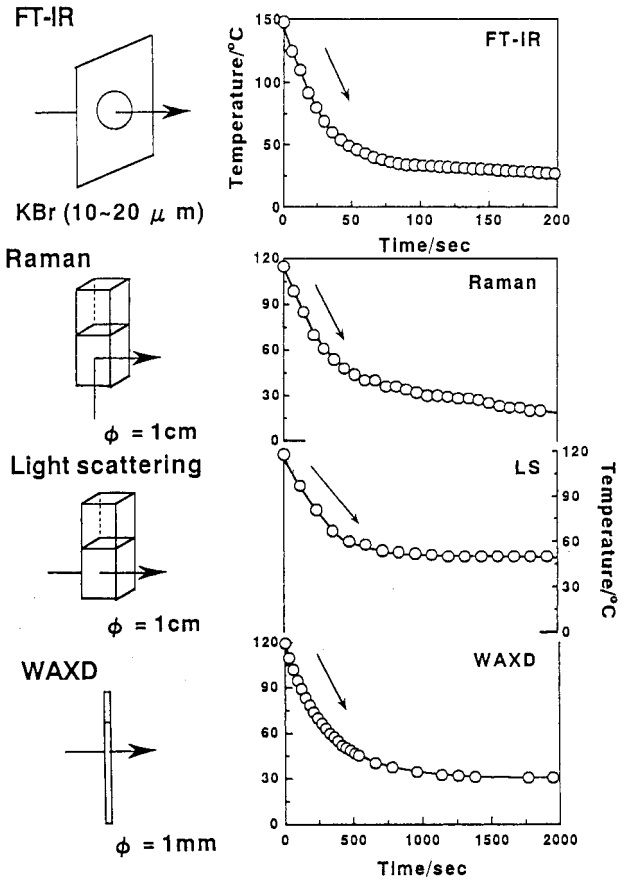

Figure 1. Time dependence of temperature decrease in cells after quenching solution to room temperature.

was detected every 6 s. Raman spectra were also measured by using an NR-1800 Raman spectrometer from Japan Spectroscopic Co., Ltd., to study the gelation process under the cooling process.

The change in the Raman spectra was detected every 90 s.

Here, we must check the time dependence of temperature in the cells used in the different measurements, since the gel formation process is very sensitive to the temperature under the cooling process. To justify the analysis of a series of experimental results, we checked a change in temperature in each sample cell as a function of time by using a temperature sensor. Figure 1 shows the results. Cells with the same diameter were used for light-scattering and Raman measurements. Namely, the diameter of the cell used for the Raman measurement was selected to simulate the temperature change in the cell used for light-scattering measurement. The change in temperature in each cell was represented, when the solutions for light-scattering and Raman measurements were quenched to 50 and 20 °C, respectively. The cell thickness for the IR spectral measurement was obliged to be thin, ca. 20 μm. Consequently, the temperature decrease by quenching was very rapid in the IR cell compared with the other cases mentioned above. Such large difference in temperature change was carefully taken into consideration in the analysis of the gelation mechanism of UHMWPP.

The thermal behavior of gel was estimated in terms of melting endotherms of DSC curves. A wet gel was placed in a standard aluminum sample pan and heated at 160 °C for 5 min. The pan was cooled to 50 °C immediately and maintained for the desired time at 50 °C to trace the time dependence of the gelation. To measure the melting point, the gels were heated at a constant rate of 10 °C min^{-1}.

To obtain the gelation temperature (T_{gel}), a test tube containing UHMWPP solution was tilted after standing for 1 h in a hot oven at a constant temperature. When the meniscus was deformed but the specimen did not flow under its own weight, we judged that the solution had gelled. This technique was adopted to judge the formation of macroscopic gels.

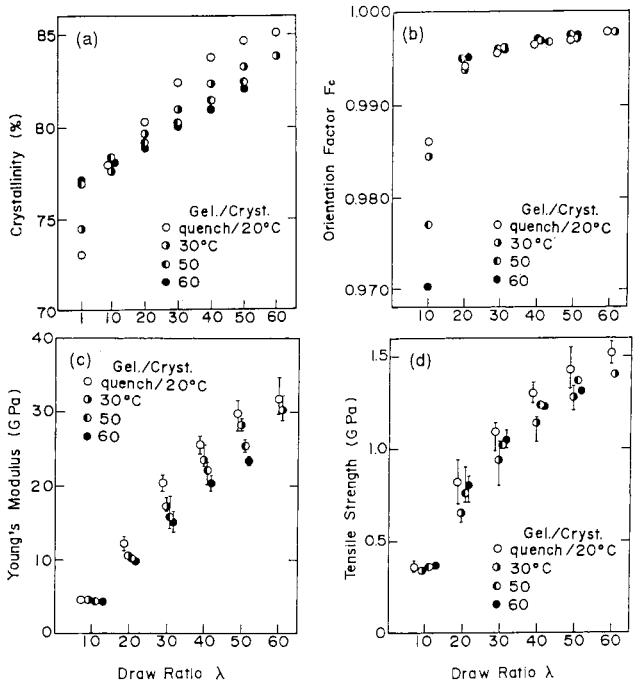

Figure 2. Change in crystallinity, orientation factor, Young's modulus, and tensile strength of the UHMWPP films with increasing draw ratio λ.

Results and Discussion

Morphology and Mechanical Properties of UHMWPP Dry Gel Films. Before discussing the experimental data concerning the gel formation, the structure and deformation mechanism of the resultant dried gel films will be discussed at first in this section to clarify the relationship between the gel formation mechanism and the drawability of the resultant dried gel films. Figure 2, parts a−d, shows the change in crystallinity, the second-order orientation factor, Young's modulus, and tensile strength of UHMWPP dry gel films with increasing the draw ratio λ. In Figure 2b, the second-order orientation factor (FC) of the *c*-axis was listed as a function of λ. FC characterizes the orientation distribution of the *c*-axis, with variation between $-1/2$ and 1.[22] For random orientation FC is 0, while for complete orientation parallel and perpendicular to the drawing direction FC is unity and $-1/2$, respectively. The FC was estimated from the three orientation factors of the (110), (040), and (130) planes based on the method of Roe and Krigbaum.[23] An increase in FC of the specimen quenched at 0 °C and dried at 20 °C is most significant at $\lambda = 10$, while the factor at $\lambda > 10$ is almost independent of gelation/crystallization temperature. The decrease in FC at initial draw ratio of $\lambda = 10$ at elevated temperature is due to the decrease in the suitable number of entanglements within the undrawn film. In Figure 2c, Young's modulus is shown as a function of λ for the gel films dried at the indicated temperature. The increase in Young's modulus with increasing λ beyond 30 times is the most significant for the film quenched at 0 °C and dried at 20 °C, and its crystallinity is the highest among specimens with $\lambda \geq 30$, indicating that the specimens with the same orientation factor may have different Young's moduli, depending on the different crystallinities. This indicates that the decrease in initial entangle-

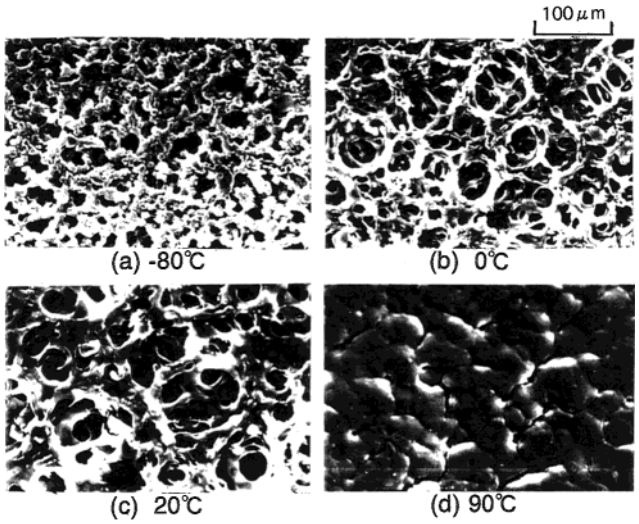

Figure 3. Change in appearance of UHMWPP films prepared by quenching solutions at the indicated temperature and by drying at 20 °C under scanning electron microscopy.

ment density due to an increase in the gelation/crystallization temperature causes an unfavorable effect on Young's modulus of the drawn films. This supports that the number of entanglements in the gels remains in the resultant dry gel films. In Figure 2d, the tensile strength increases with draw ratio but the magnitude is almost independent of gelation/crystallization temperature except for the specimens quenched at 0 °C and dried at 20 °C. This indicates that the tensile strength is sensitive to the inner stress concentration occurred around defects such as cracks rather than the number of entanglements.

Here it should be noted that when the hot homogenized solution was quenched to temperatures beyond 80 °C, the draw ratio of the resultant dry gel film was less than 10 times. Incidentally, our preliminary experiments provided that the drawability of the resultant dry gel films is hardly affected by the cooling rate of the solutions in contrast with small influence of cooling temperature to the drawability.

Figure 3 shows the change in appearance of UHMWPP films viewed under scanning electron microscopy (SEM). The samples were prepared by quenching solutions at the indicated temperature and followed by drying at 20 °C. The continuous fibrillar texture shows honeycomblike structure, the size of the holes becoming smaller as the quenching temperature decreases. Observation reveals that honeycomblike structure comprised interconnected lamellar crystals. Micrograph d shows the morphology of the film cast at 90 °C. Spherulitic structure could be observed instead of the fibrous structure shown in micrographs a−c. This is the typical morphology observed for melt-crystallized films. Despite the drastic changes of fibrous structure, the crystallinity decreased slightly from 76.5 to 73.5% as the quenching temperature was lowered from +90 to −80 °C. Incidentally, small-angle light-scattering patterns from specimens a−c under Hv polarization condition were X-type, indicating the existence of rodlike textures, the optical axes being oriented parallel or perpendicular to the rod axis.[24] The pattern from specimen d was the so-called "four leaf clover pattern" indicating the scattering from spherulites.[25]

Figure 4 shows the morphology of the drawn specimens at $\lambda = 2$, in which parts a−c reveal that the cross-

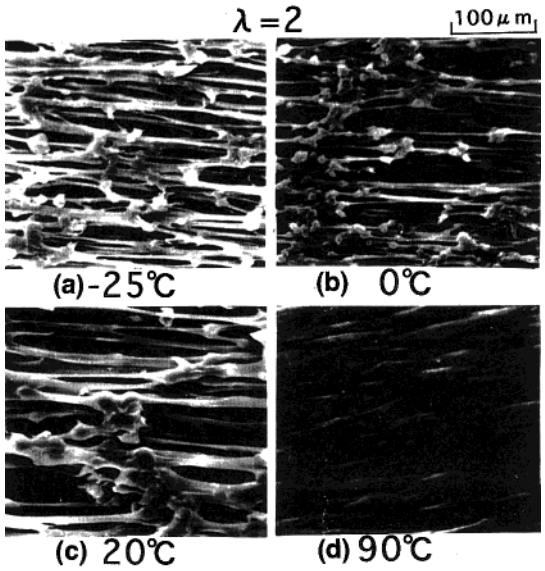

Figure 4. Scanning electron micrographs of the specimens with $\lambda = 2$, in which the films were prepared by quenching solutions at the desired temperatures and by drying at room temperature.

linking loci appeared to consist of fibrillar shish-kebab-like structures which were arranged in the drawn direction. In contrast, micrograph d shows the ellipsoidal structure indicating the deformation of spherulite. The successful elongation could be done up to $\lambda = 60$ for morphologies a−c, while the maximum elongation of the films cast at 90 °C was less than 10 times. The morphology in Figures 3 and 4 indicates that the network structure showing honeycomblike structure plays an important role in ensuring high drawability, since inner stress within the film is transmitted smoothly in the stretching direction. Accordingly, the greatest drawability of the dry gel films is attributed to two factors. One is a reduced number of entanglement meshes per molecule in solution−cast/spun polymers.[2] The other is the continuous fibrillar texture showing honeycomblike structure. The dense network structure plays an important role in ensuring significant drawability in order to transmit inner stress smoothly in the stretching direction.

Here it may be noted that the significant drawability and mechanical properties are affected by gel formation process sensitive to quenching temperature of the solutions. Accordingly, the time dependence of the isothermal phase separation of the UHMWPP solutions is estimated in relation to the gelation mechanism by using elastic light scattering, X-ray, and optical microscopy.

Gelation Process of UHMWPP Solutions Observed by Elastic Light Scattering. Figure 5 shows the change in the logarithm plots of the scattered intensity against time at various q observed in the gelation process of the 1.0% solutions, where the magnitude of the scattering vector is given by $q = (4\pi n/\lambda')\sin(\theta/2)$, λ', θ, and n being the wavelength of light in solution, the scattering angle, and the refractive index of solvent, respectively. The refractive index n was carefully measured by an Atago-2T index meter (Atago Co. Ltd.). The same measurements were done for 0.9−1.3% solutions at temperatures $< T_{gel}$ determined for each concentration in the preliminary experiments. As can be seen in Figure 5, the logarithm of the scattered

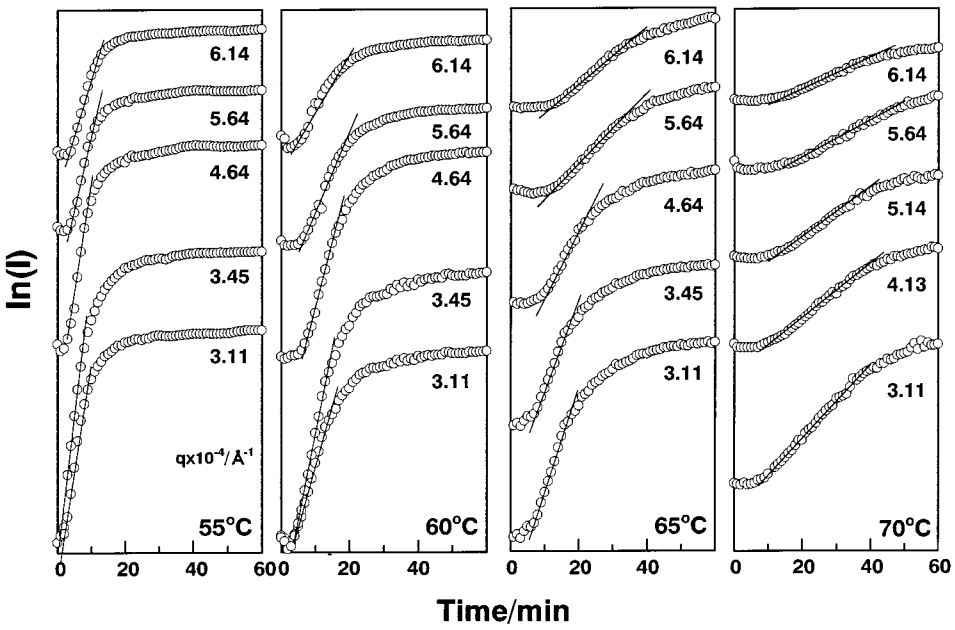

Figure 5. Logarithm plots of the scattered intensity against time at various q observed for 1.0% solutions.

intensity increased linearly with time in the initial stage of phase separation, indicating the possibility of successful analysis with the linear theory of spinodal decomposition by Cahn.[26] With time, the logarithm of scattered intensity tends to deviate from the linear relationship, as has been observed for the later stage of spinodal decomposition of amorphous polymer blends.[27−28] The deviation shifts to shorter time scale as the temperature increases. If the linear relationship reflects the initial stage of spinodal decomposition as pointed by Cahn,[26] it is well-known that the change in scattered intensity in Figure 4 can be given by

$$I(q,t) = I(q,t=0)\exp[2R(q)t] \qquad (1)$$

where $I(q,t)$ is the scattered intensity at the time t, after initiation of the spinodal decomposition, and $R(q)$ is the growth rate of concentration fluctuation given as a function of q

$$R(q) = -D_C q^2\left\{\frac{\partial^2 f}{\partial c^2} + 2\kappa q^2\right\} \qquad (2)$$

where D_C is the translational diffusion coefficient of the molecules in the solution, f is the free energy of mixing, c is the concentration of the solution, and κ is the concentration-gradient energy coefficient defined by Cahn and Hilliard.[29] A linear relationship in the plot of ln(I) vs t at fixed q was also obtained for UHMWPP solutions with other concentrations at various temperatures.

A question can arise as to whether phase separation of UHMWPP is attributed to the spinodal decomposition, if the linear relationship depicted in Figure 5 can be observed. Figure 6 shows the growth rate of concentration fluctuation $R(q)$ plotted against q for the 0.9 ∼ 1.3% solutions. The maximum growth rate $R(q_m)$ increases and the value of the corresponding scattering vector, q_m, shifts slightly toward wider angle or maintains at the same angle with decreasing measured temperature T. This phenomenon is in good agreement with the principle of spinodal decomposition for amorphous polymer solutions proposed by van Aartsen,[30] if

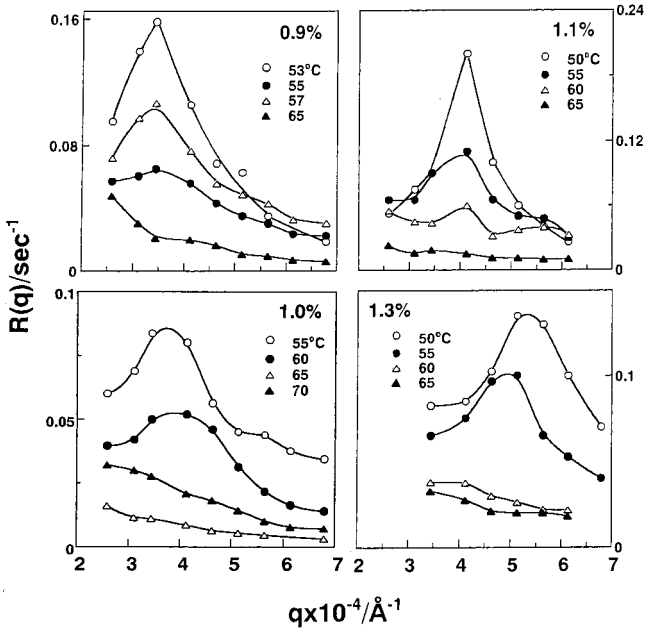

Figure 6. Growth rate of concentration fluctuation $R(q)$ plotted against q for the 0.9 ∼ 1.3% solutions.

the spinodal temperature T_S is higher than 70 °C. Namely, his theory pointed out that the value of q_m increases with increasing temperature difference ($T_S - T$), if the range of molecular interaction associated with the mean square radius of gyration based on the concept of Debye et al.[31] is independent of temperature. Accordingly, the shift of $R(q_m)$ to a higher value on increasing the difference ($T_S - T$) justified the analysis of the linearized theory of the spinodal decomposition.[26]

Figure 7 shows the evolution of scattered light intensity of the 1% solution plotted against q at the indicated time. The measurements were done at 50 °C. To obtain the quantitative results, the correction of scattered intensity from the solution was made for absorption and the obtained intensity was plotted after subtracting the intensity scattered from the solvent. With increasing time, the scattering peak becomes higher, but the scattering peak is at the same position.

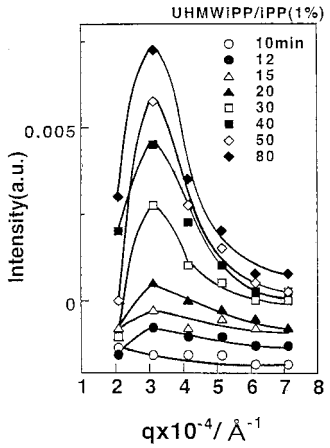

Figure 7. Scattered intensity of light plotted against q measured for the 1% solution at the indicated time.

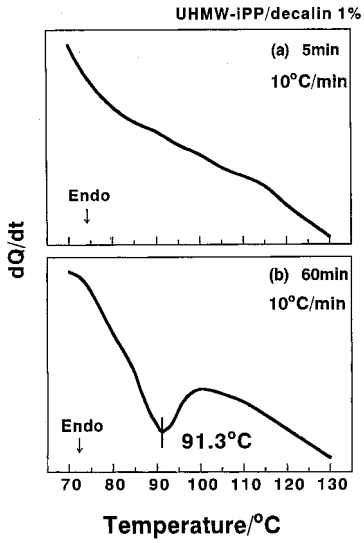

Figure 8. Change in DSC thermograms measured for gels prepared from 1% solution at the indicated time. Parts a and b correspond to data obtained at two different times after the start of the experiment.

This is surely one of the characteristic phenomena indicating spinodal decomposition. Such a phenomenon was reported for the gelation of poly(vinyl alcohol).[32] From the scattering peak, the periodic structure characterizing spinodal decomposition can be estimated to be 2 μm.

Columns a and b in Figure 8 show the change in the profile of the DSC curves for gels prepared from 1% solution at the indicated time. Two columns correspond to data obtained at two different times after the start of the experiment. The two different times can be related to the experiments in Figure 5. Namely, the sample used for the DSC measurement was the same as that used for ln(I) vs time measured by quenching the solution to 65 °C shown in Figure 5d. As shown in Figure 5d, 5 min in Figure 8a corresponds to the time ensuring the linear relationship, while 60 min corresponds to time associated with the deviation from the linear relationship between ln(I) and time. The solution concentrations shown in Figure 8 were confirmed from the difference of weight of gels under DSC measurement by considering evaporation of solvent from gels at elevated temperature. Here it should be noted that no endotherm peak was observed at initial stage (5 min), while a clear peak was observed at 91.3 °C for gels after the reaction progressed for 60 min. This means that 5 min is the initial stage of the phase separation associated with appearance of polymer-rich phase, while 60 min is the later stage of the phase separation associated with formation of ordered structures within the polymer-rich phase. The ordered structure is speculated to be aggregation of crystallites grown with the progression of time, although the endotherm peak at 91.3 °C for the gels is much lower than that (167−170 °C) of crystallites within UHMWPE dry gel film. The large difference between the peak temperatures is only attributed to the dissolution of crystallites in decalin solvent. The experimental investigation of the formation of crystallites in the gel will be made in a later section.

Table 1. Spinodal Decomposition (SD) Temperatures of UHMWPP Solutions with Various Concentrations

concn (%)	SD temp (°C)
0.9	71.4
1.0	75.4
1.1	75.8
1.2	76.7

Table 2. Values of D_{app} of UHMWPP Solutions with Various Concentrations[a]

	concentrations (%)			
temp (°C)	0.9	1.0	1.1	1.3
50				−0.417
53	−0.560	−0.509		
55	−0.440		−0.410	−0.335
57	−0.345	−0.346		
60		−0.250	−0.320	−0.250
65	−0.180	−0.168	−0.218	−0.190

[a] Units: $D_{app} \times 10^{-13}$cm^2/s

On the basis of a series of experimental results, the spinodal temperature, T_S, was estimated for UHMWPP solutions to pursue the detailed discussion according to the linear Cahn theory.[26] The treatment was described in a previous paper in detail.[33] Table 1 shows the values of T_S at various concentrations, and Table 2 lists the values of D_{app} ($=D_c(\partial^2 f/\partial c^2)$). The values of D_{app} are efficiently estimated by obtaining an intercept at $q^2 = 0$ in the plot $R(q)/q^2$ vs q^2 by assuming pure spinodal decomposition. Because of the positive values of D_c by definition, the negative values of D_{app} characterizes unstable regions associated with spinodal decomposition. The small values of $\partial^2 R(q)/\partial q^2|_{q=q_m}$; hence, $D_{app}(\partial^2 R(q)/\partial q^2|_{q=q_m} = 8D_{app})$, indicate no appearance of a clear scattering ring at the later stage of spinodal decomposition. To observe a distinct scattering maximum in the linear spinodal decomposition regime, it is evident that the value of D_{app} must be usually 3 or 4 orders of magnitude greater.

Here it is seen that the spinodal temperature, T_S, listed in Table 1 shifts to higher value as the concentration of solution increases. The spinodal temperature, T_S, of the UHMWPP solution is higher than those of atactic-PVA (at-PVA) and syndiotactic-PVA (st-PVA) solutions.[33] Even so, no $H\nu$ scattering pattern from UHMWPP solution can be observed in the later stage which deviates from the linear relationship in Figure 5, although X-type patterns under $H\nu$ polarization condition could be observed in the initial stage of the phase separation of at- and st-PVA solutions. This phenomenon is due to the fact that UHMWPP with no hydrogen bonds causes much more significant effect on the progression of phase separation associated with spinodal decomposition than the cases of at- and st-PVA. In other

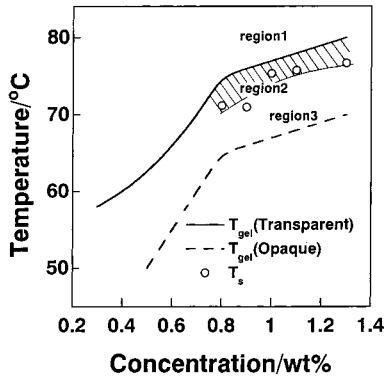

Figure 9. Phase diagram concerning the concentration dependence of spinodal temperature, T_S, and gelation temperature.

words, the gelation of at- and st-PVA solutions is associated with the rapid appearance of the aggregation of stable crystallites in the initial stage of the phase separation.

Figure 9 shows a phase diagram concerning the concentration dependence of spinodal temperature (T_S) and gelation temperature (T_{gel}). Spinodal decomposition temperature was represented by solid circles, while the solid and dashed curves correspond to the temperatures where the transparent and opaque gels were detected, respectively. The appearance of turbid gels is associated with crystallization. The sol−gel transition cannot occur above the solid curve, while the gelation rate becomes faster as the temperature decreases below the solid curve. The phase separation can be classified into three regions: a homogeneous sol region (region 1), a gel region between the solid curve and spinodal decomposition point (region 2), and a gel region under the spinodal decomposition point indicating simultaneous advance of both gelation and spinodal decomposition (region 3). Region 2 is independent of the liquid−liquid phase separation. A question can arise whether the phase diagram is useful to understand the detailed mechanism of phase separation of UHMWPP solutions. Actually, the gelation temperature was determined after keeping the solution for 1 h, while the spinodal decomposition temperature is defined in the initial stage of spinodal decomposition which corresponds to a shorter time scale than 1 h as shown in Figure 5. If the gelation was defined at such a time scale that the plots of ln(I) vs time starts to deviate from the linear relationship as shown in Figure 5, the gelation temperature becomes lower than the solid curve in Figure 9. Of course, the existence of partial gels was observed in the solution on the above time scale. In the case, the gelation temperature is postulated to be almost equal to the spinodal temperature indicating simultaneous advance of both gelation and spinodal decomposition.

Figure 10 shows an optical micrograph of the gels. The 1% UHMWPP solution in a dish was quenched from 150 to 20 °C. Namely, the dish was put on the optical stage set at 20 °C. The photograph was taken after 150 min. The continuous tissue showing three-dimensional networks can be observed with a periodic period of 10 μm. This size is larger than the characteristic wavelength 2 μm estimated from the evolution of scattered intensity plotted against q (see Figure 7). One of the reasons is probably due to the different sample preparation condition such as sample thickness and gelation time. The another reason is thought to be due to the

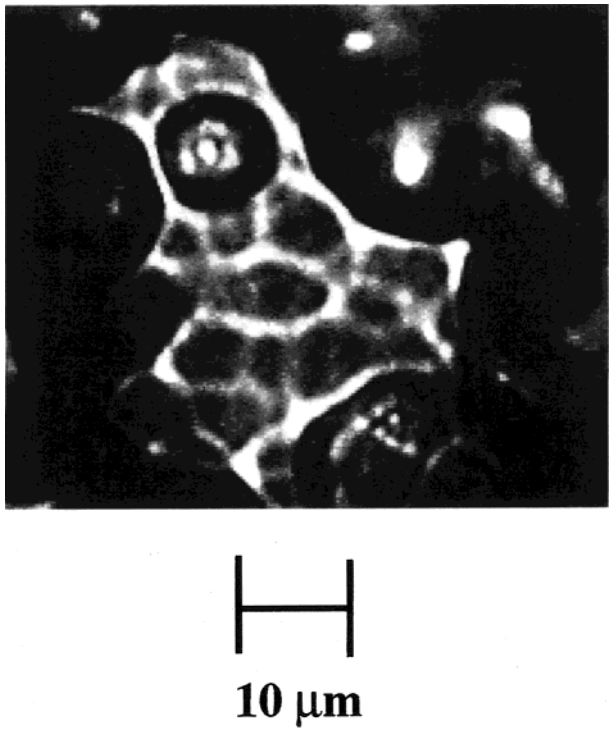

Figure 10. Optical micrograph of the gels. The photograph was taken at 150 min after the solution was quenched to 20 °C.

fact that crystallization of UHMWPP chains in the polymer-rich phase forms the rigid networks and the holes become inevitably bigger with the progression of the crystallization because of the shrinkage of the polymer-rich phase. Anyway, the confirmation of the continuous tissue with the periodic structure indicates that gelation of UHMWPP is associated with the liquid−liquid phase separation owing to spinodal decomposition.

Here we must emphasize that the specimens prepared by quenching the solutions at temperatures higher than the spinodal temperature listed in Table 1 and Figure 9 could not be elongated beyond 10 times. As discussed before, the orientation factor, Young's modulus and tensile strength became slightly higher with decreasing quenching temperature as shown in Figure 2. Furthermore, q_m, shifted slightly toward wider angle or maintained at the same angle with decreasing measured temperature as shown in Figure 6, indicating the slight decrease in the periodic size characterizing spinodal decomposition. Judging from the two factors, it may be expected that the dense network structure emphasizes significant drawability to transmit inner stress smoothly in the stretching direction. This indicates that the liquid−liquid phase separation is one of the important factors to ensure the significant drawability of the resultant dry gel films.

Phase Separation of UHMWPP Solutions Observed by X-ray, IR, and Raman. Returning to Figure 8, the endotherm peak at 91.3 °C suggests crystallization due to the growth of ordered structure within the polymer-rich domains in the later stage of spinodal decomposition. To justify the existence of crystallites as cross-linkages of gels, gel formation was estimated in microscopic levels by using X-ray, FT-IR, and Raman techniques. As discussed in Figure 1, the cell thickness on measuring IR spectrum is 20 μm, and the temperature decrease by quenching is very rapid but the

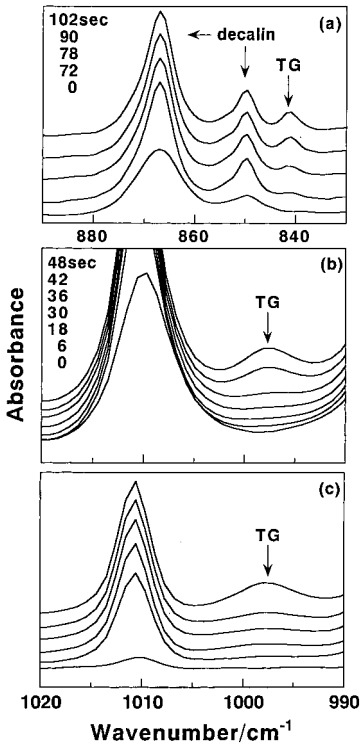

Figure 11. FT-IR spectra in the cooling process of 1% solution from 160 to 30 °C: (a) spectra in the wavenumber range from 830 to 890 cm^{-1}; (b) spectra in the wavenumber range from 990 to 1020 cm^{-1}; (c) the spectra obtained by subtracting the absorption of solvent from spectra b.

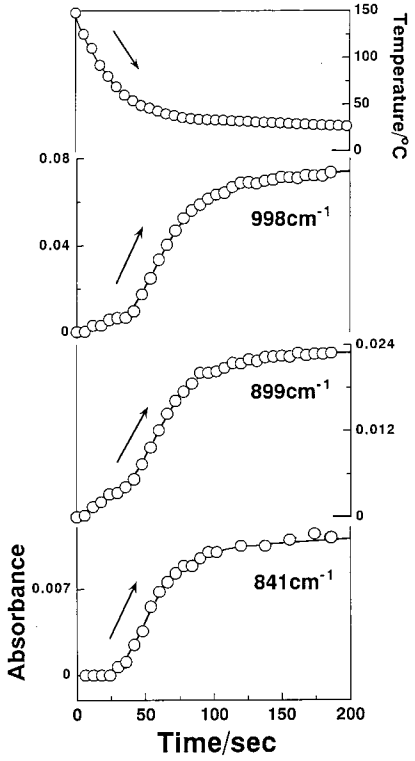

Figure 12. Time dependence of the infrared absorption band intensity at 998 and 899 cm^{-1}.

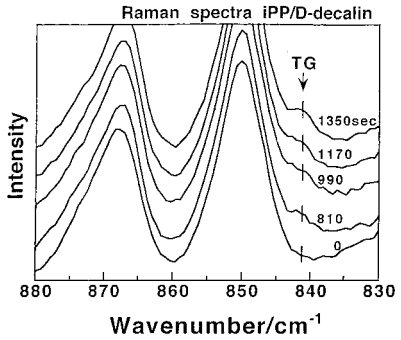

Figure 13. Raman spectra in the cooling process of 1% solution from 160 to 30 °C.

temperature decrease in other cases is not so rapid because of larger diameter of the cells. The following analysis for the gelation mechanism is carried out by considering the time dependence of temperature in each cell as shown in Figure 1.

Figure 11 shows time-resolved FT-IR spectra measured under the procees of cooling a 1% solution from 150 to 30 °C. A number of absorption peaks characterizing the TG type 3_1 helix, which are so-called crystalline sensitive bands, have been confirmed for it-PP films but most peaks except for 841, 899 and 998 cm^{-1} bands were overlapped with the peaks of decalin solvent in the present experiments.[34] Column a shows the spectra in the wavenumber range from 830 to 890 cm^{-1}. Appearance of 841 cm^{-1} band indicates the existence of the 3_1 helix. Column b concerning the spectra in the wavenumber range from 990 to 1020 cm^{-1} indicates also an appearance of 998 cm^{-1} band associated with the 3_1 helix. Column c shows the spectra obtained by subtracting absorption of solvent at 150 °C from the spectrum of column b. As shown in parts b and c, a peak associated with the helix band appeared at 30 s after quenching, namely when the cell was cooled to 30 °C (see Figure 1). The 998 cm^{-1} band became sharper with time. This indicates that the ordering of molecular chains became pronounced with time. A similar tendency was also confirmed in column a. The 841 cm^{-1} band increased in intensity with time, and this peak is also associated with the ordering of molecular conformation.

Figure 12 shows the time dependence of the absorption peak intensity of the bands at 998, 899 and 841 cm^{-1}. Temperature decreases with time and approaches 30 °C after 50 s. Around there, the intensities of the three bands increase drastically indicating that conformational ordering to form a TG type 3_1 helix is enhanced in the gelation process by the progression of the phase separation.

Figure 13 shows a Raman spectra under the process of cooling a 1% solution from 160 to 30 °C. In preliminary experiment, it was confirmed that the Raman peaks of it-PP were overlapped with those of [H]-decalin (usual solvent). To obtain as many as possible clear Raman bands of it-UHMWPP gels, [D]-decalin was used as a solvent to shift the Raman peak of solvent from that of it-PP. Here it should be noted that the gel obtained for the it-UHMWPP in [D]-decalin behaves essentially in the same manner with the gel obtained for a normal [H]-decalin solution. The crystalline band can be observed at 841 cm^{-1} as in the case of IR spectra (see Figure 11), though it is less distinct than the corresponding IR band. Hence the accumulation was taken for a long time under a lower resolution condition to obtain a high signal-to-noise ratio. The band becomes clearer beyond 810 s, indicating the growth of ordered conformation at temperatures lower than 45 °C (see Figure 1).

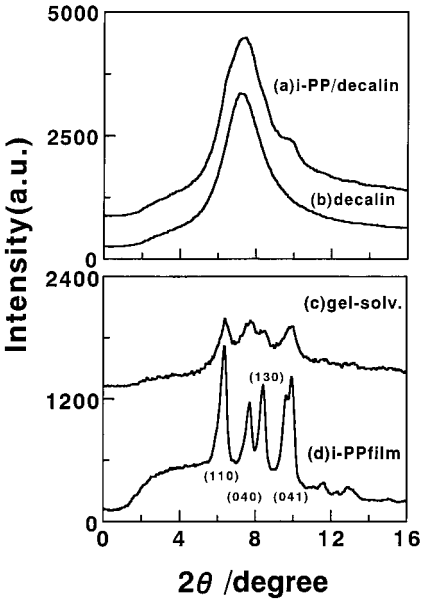

Figure 14. X-ray diffraction profiles obtained for UHMWPP gel: curve a, the gel at 20 °C; curve b, decalin solution; curve c, curve a − curve b; curve d, dry gel film. The incident X-ray beam was the Mo Kα line.

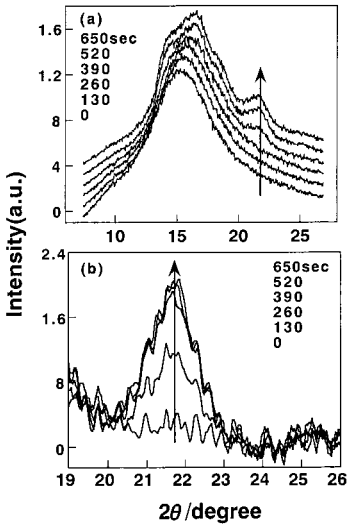

Figure 15. (a) Time evolution of X-ray diffraction profile measured for 1% solution quenched to 30 °C and (b) the diffraction curve after subtracting the scattering from solvent.

Figure 14 shows the X-ray diffraction profile obtained for the gel, where the measurement was done at 1 h after the 1% solution was quenched from 150 to 30 °C. Curve a shows the diffraction profile from the 1% solution and curve b that from decalin solution. The shoulder around $2\theta = 10°$ indicates the existence of crystallites within the gels. Curve c shows the diffraction of gels after subtracting the scattering from solvent. The diffraction peaks from the (110), (040), (130), and (041) planes could be observed clearly. Comparing curve c with curve d of the dry gel film, the growth of crystallites under gelation process is evident.

Figure 15 shows the time evolution of the X-ray diffraction intensity obtained in the gelation process. In this measurement the Cu Kα line was used as an incident beam and the scattering angles are different from those in Figure 14 with the Mo Kα beam. Column a shows the diffraction curves for 1% solution quenched from 160 to 30 °C, and column b shows the diffraction

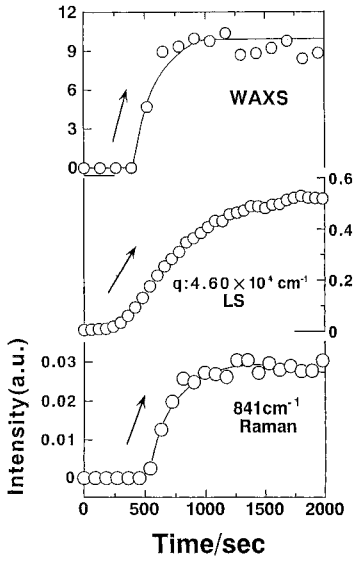

Figure 16. Comparison of time dependence of intensity among X-ray, light-scattering, and Raman data.

curves obtained after subtracting the scattering from solvent. The measurements were carried out immediately after quenching the solution and the accumulation time of X-ray intensity was 130 s. A broad peak from the (041) plane could be detected clearly in the time region beyond 350 s.

In Figure 16, the time evolutions of scattering intensity observed for light scattering, X-ray and Raman are compared with each other. This comparison can be made because the time dependence of temperature in each cell is almost the same as shown in Figure 1. The X-ray intensity was evaluated for the (041) reflection. Raman intensity was estimated for the 841 cm^{-1} band. The scattered intensity of He−Ne gas laser was detected at $q = 4.13 \times 10^{-4}$Å^{-1}. The scattered light intensity was found to rise up in the time region of ca. 300 s. This is faster than the rising-up time of intensities detected by X-ray diffraction. The increase in intensity of X-ray, IR, and Raman is associated with an increase in crystallinity within the gels, while the increase in the light-scattering intensity corresponds to the progression of the phase separation. This indicates that at a temperature >50 °C, the progression of crystallization is not significant during the progression of phase separation and the crystallization in the polymer-rich phase is pronounced with time (see the DSC curves in Figure 8). Accordingly, it may be expected that when UHMWPP solution is quenched to T_S (see Table 1), the phase separation associated with spinodal decomposition occurs at first and the crystallization occurs in the polymer-rich phase subsequently. On the other hand, solution was quenched at temperature much lower than T_S, phase separation and crystallization occur simultaneously.

To confirm the existence of crystallites as cross-linking points of the gels, the dissolution behavior of gels was estimated by DSC, WAXD, light-scattering, and FT-IR measurements. The results are shown in Figure 17. As estimated by DSC, the crystallinity decreased drastically around melting point (91.3 °C). The IR absorption intensity of the 998 cm^{-1} band and the X-ray intensity from the (041) plane decreased in the temperature region of partial melting of crystallites confirmed by DSC measurement. On the other hand, light-scattering intensity increased above 85 °C or even

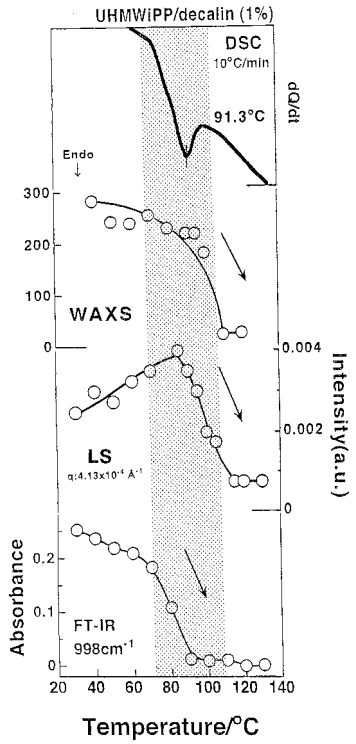

Figure 17. Dissolution behavior of gels estimated by DSC, WAXD, light-scattering, and FT-IR measurements.

in the temperature region of the partial melting of crystallites and decreased beyond 90 °C. This indicates that the periodic continuous structure characterizing spinodal decomposition of the solutions was maintained despite the partial melting of crystallites.

Morphology and Mechanical Property of UHMWPP Gels at an Equilibrium State. To postulate the morphology of gels at an equilibrium state, light-scattering measurement under polarization conditions is one of the most useful tools. Under an *Hv* polarization condition, no light scattering could be observed. Only an indistinct circular pattern with very weak intensity was observed without azimuthal angle dependence, indicating the formation of random array crystallites smaller than the wavelength of the incident beam or a random orientation fluctuation of optical axes within polymer-rich phase even in the later stage of phase separation. On the basis of this result, the *Vv* scattering from UHMWPP gels was found to be due to a correlation concerning fluctuation in average polarizability.[35] Then, we have

$$I_{Vv} - \frac{4}{3}I_{Hv} = K\langle\eta^2\rangle \int_0^\infty \gamma(r)\,\frac{\sin qr}{qr}\,r^2\,\mathrm{d}r \qquad (3)$$

where $\langle\eta^2\rangle$ is the mean-square polarizability fluctuation and $\gamma(r)$ is the corresponding correlation function. In the present study, the angular dependence of scattered intensity is a monotonically decreasing function. Such a monotonic intensity distribution suggests the difficulty in obtaining $\gamma(r)$ by a Fourier transformation with sufficient accuracy, and the desired information could be extracted by approximating $\gamma(r)$ as a Gaussian function.[36]

$$\gamma(r) = \exp\left(-\frac{r^2}{a^2}\right) \qquad (4)$$

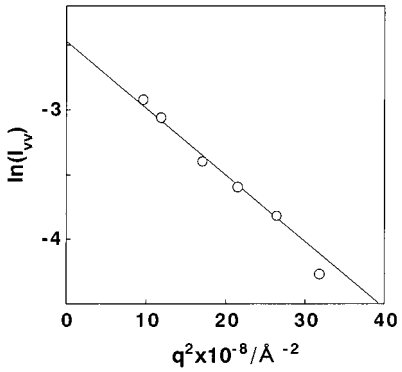

Figure 18. Scattered intensity data plotted as the logarithm of the absolute Rayleigh ratio vs q^2 for UHMWPP whiten gels at 50 °C.

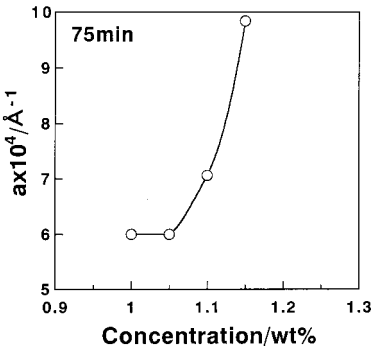

Figure 19. Concentration dependence of the correlation length *a*, measured at 50 °C for gels after keeping for 75 min.

Substituting eq 4 into eq 3 and performing the integration yields

$$\ln\left(I_{Vv} - \frac{4}{3}I_{Hv}\right) = \ln\left(\frac{16}{\lambda^4}\pi^{11/2} <\eta^2> a^3\right) - \frac{a^2}{4}q^2 \qquad (5)$$

Parameter *a* is the correlation length estimating the extension of the inhomogeneities.[36−37] The gel becomes uniform when *a* takes an infinite value.

Figure 18 shows an example of scattered intensity data plotted as the logarithm of the absolute Rayleigh ratio vs q^2 for UHMWPP whiten gels at 50 °C. The slope of the line allows the determination of the parameter a in eq 5 and by extrapolation to zero angle the quantity $\langle\eta^2\rangle$ is obtained.

Figure 19 shows the concentration dependence of parameter *a*, which was measured for gels after keeping them for 75 min at 50 °C. The measurement was done for the solutions whose concentration was in the range 1.0−1.15%. Actually, the gels became uniform with increasing concentration beyond 1.0% at the later stage of the phase separation. The value of the correlation length, *a*, increases drastically with increasing concentration. This increase means the progression of the phase separation of the UHMWPP solution. In contrast, when the gels with concentrations lower than 1.0% were set at 50 °C for more than 1 day, clear microsyneresis could be observed, and the gels beyond 1.2% concentration became stiffer drastically and microsyneresis could be observed.

Conclusion

The morphology and mechanical properties of the UHMWPP films that were prepared by quenching the solutions and followed by evaporation of the solvents

could be related to the characteristics of the phase separation of UHMWPP solutions. Under SEM, the tissue in the film was observed to take a honeycomblike structure, whose hole size became smaller as the quenching temperature decreased, but the size distribution was narrow. The dense network structure plays an important role in ensuring significant drawability in order to transmit inner stress smoothly in the stretching direction.

To facilitate understanding of the formation of such network structure, the phase separation in the gelation process was studied by light-scattering technique. The logarithm of scattered intensity against time yielded a straight line and started to deviate from this linear relationship in the stage. No appearance of anisotropic rods even in the later stage could be observed by light scattering under Hv polarization condition for UHMWPP gels with concentrations < 20%. The maximum growth rate $R(q_m)$ of concentration fluctuation increased with decreasing temperature and the value of the scattering vector, q_m, shifted slightly toward higher scattering angle or maintains at the same angle with increasing difference ($T_S - T$) between the measurable temperature, T, and spinodal temperature T_S. These phenomena were in good agreement with the principle of spinodal decomposition.

The crystallization within the gels was confirmed by X-ray, IR, and Raman measurements. Namely, the X-ray diffraction intensity from the (041) plane and the intensity of the crystallization-sensitive IR and Raman bands increased drastically in the gelation process. These data, in addition to those given in Figure 17, confirmed that the crystalline structure plays as cross-linkages of the gels. The increase in intensity of light scattering was faster than the increases in intensities measured by X-ray diffraction and Raman scattering, indicating more predominant progression of spinodal decomposition rather than crystallization. Accordingly, it may be concluded that when UHMWPP solution is quenched, the liquid−liquid phase separation associated with spinodal decomposition occurs at first and the crystallization occurs subsequently in the polymer-rich phase.

References and Notes

(1) Smith, P.; Lemstra, P. J. *J. Mater. Sci.* **1980**, *15*, 505.
(2) Smith, P.; Lemstra, P. J.; Booij, H. C. *J. Polym. Sci., Polym. Phys. Ed.* **1981**, *19*, 877.
(3) Smith, P.; Lemstra, P. J.; Pippers, J. P. L.; Kiel, A. M. *Colloid Polym. Sci.* **1981**, *258*, 1070.
(4) Matsuo, M.; Inoue, K.; Abumiya, N. *Sen-I-Gakkaishi* **1983**, *36*, 696.
(5) Matsuo, M.; Sawatari, C.; Iida, M.; Yoneda, M. *Polym. J.* **1985**, *17*, 1975.
(6) Matsuo, M.; Sawatari, C.; Nakano, T. *Polym. J.* **1986**, *18*, 759.
(7) Sawatari, C.; Matsuo, M. *Macromolecules* **1989**, *22*, 2968.
(8) Ogita, T.; Kawahara, K.; Soga, K.; Matsuo, M. *Polymer* **1992**, *33*, 698.
(9) Kobayashi, M.; Nakaoki, T.; Ishihara, N. *Macromolecules* **1990**, *23*, 78.
(10) Kobayashi, M.; Kozasa, T. *Appl. Spectrosc.* **1993**, *47*, 1417.
(11) Kobayashi, M. *Macromol. Symp.* **1997**, *114*, 1.
(12) Tan, H.-M.; Moet, A.; Hilter, A.; Bear, E. *Macromolecules* **1983**, *16*, 28.
(13) Gan, J. Y. S.; Francois, J.; Guenet, J.-M. *Macromolecules* **1986**, *19*, 173.
(14) Klein, M.; Guenet, J.-M. *Macromolecules* **1989**, *22*, 3716.
(15) Klein, M.; Brulet, A.; Guenet, J.-M. *Macromolecules* **1990**, *23*, 540.
(16) Guenet, J.-M. *Macromolecules* **1986**, *19*, 1961.
(17) Boyer, R. F.; Bear, E.; Hiltner, A. *Macromolecules* **1985**, *18*, 427.
(18) Izumi, M.; Suzuki, J.; Katano, S.; Funahashi, S. *Physica B* **1995**, *213&214*, 724.
(19) Tashiro, K.; Joubert, F.; Fukuda, K.; Kaneko, F. *Polym. Prepr. Jpn.* **1998**, *47*, 3811.
(20) Matsuo, M.; Sawatari, C. *Macromolecules* **1986**, *19*, 2036.
(21) Ogita, T.; Yamamoto, R.; Suzuki, N.; Ozaki, F.; Matsuo, M. *Polymer* **1991**, *32*, 822.
(22) Hermans, P. H. *Physics and Chemistry of Cellulose Fibers*; Elsevier: New York, 1949; Chapter 5.
(23) Roe, R. J.; Krigbaum, W. R. *J. Chem. Phys.* **1964**, *40*, 2608.
(24) Rhodes, M. B.: Stein, R. S. *J. Polym. Sci., Part B* **1963**, *1*, 663.
(25) Stein, R. S.; Rhodes, M. B. *J. Appl. Phys.* **1960**, *31*, 1873.
(26) Cahn, J. W. *J. Chem. Phys.* **1965**, *42*, 93.
(27) Hashimoyo, T.; Kumaki, J.; Kawai, H. *Macromolecules* **1983**, *16*, 641.
(28) Hashimoyo, T.; Sasaki, K.; Kawai, H. *Macromolecules* **1984**, *17*, 2812.
(29) Cahn, J. W.; Hilliard, J. E. *J. Chem. Phys.* **1958**, *29*, 258.
(30) van Aartsen, J. *J. Eur. Polym. J.* **1970**, *6*, 919.
(31) Deby, P.; Chu, B.; Woermann, D. *J. Chem. Phys.* **1962**, *36*, 1803.
(32) Kanaya, T.; Ohkura, M.; Takeshita, H.; Kaji, K.; Furusaka, M.; Yamaoka, H.; Wignall, G. D. *Macromolecules* **1995**, *28*, 3168.
(33) Matsuo, M.; Sugiura, Y.; Takematsu, S,; Ogita, T.; Sakabe, T.; Nakamura, R. *Polymer* **1997**, *38*, 5953.
(34) Stein, R. S.; Wilson, P. R. *J. Appl. Phys.* **1962**, *33*, 1914.
(35) Tadokoro, H.; Kobayashi, M.; Ukita, M.; Yasufuku, K.; Marahashi, S.; Torii, T. *J. Chem. Phys.* **1965**, *42*, 4.
(36) Deby, P.; Bueche, A. M. *J. Appl. Phys.* **1949**, *20*, 518.
(37) Pines, E.; Prins, W. *Macromolecules* **1973**, *6*, 888.

MA011402+